processes

MDPI

Article

A Laboratory-Scale Numerical Investigation of the Effect of Confinement Conditions on the Mechanical Responses of Coal under Various Saturation Conditions

Huping Wang [1,2], Zhao Wang [3], Sanqing Ding [1,*], Chao Jin [4], Xiaogang Zhang [4] and Langtao Liu [4]

[1] School of Public Policy & Management, China University of Mining and Technology, Xuzhou 221116, China
[2] School of Marxism, Hebei University of Engineering, Handan 056038, China
[3] School of Management Engineering and Business, Hebei University of Engineering, Handan 056038, China
[4] Hebei Collaborative Innovation Center of Coal Exploitation, Hebei University of Engineering, Handan 056038, China
* Correspondence: 0234@cumt.edu.cn

Abstract: Deep coal seams are generally preferred for CO_2 sequestration, during which the saturation fluids and high-stress condition involved can significantly alter the mechanical attributes of coal. To understand the effect of stress conditions on the mechanical properties of coal during CO_2 sequestration, a finite element model was developed and subsequently validated using experimental data. The results indicate that coal strength increases from 10.35% for a 5 MPa CO_2-saturated sample to 114.54% for an 8 MPa CO_2 + water-saturated sample as the confining pressure rises from 0 to 30 MPa, due to reduced porosity. However, this effect diminishes with higher confining pressures as dilation decreases. The critical confining pressure determined in this study is approximately 20 MPa, at which all samples exhibit similar failure strength (around 48.50 MPa). Moreover, the strengthening effect caused by applied stress is especially pronounced in CO_2-saturated samples, particularly in those saturated with super-critical CO_2 and CO_2 + water. This suggests that the reduction in coal strength resulting from the adsorption of saturation fluids can be counterbalanced by the strength gain resulting from applied stress. The aforementioned results highlight the effectiveness of injecting high-pressure super-critical CO_2 into deep coal seams for carbon sequestration purposes.

Keywords: CO_2 sequestration; deep coal seams; numerical simulation; effective stress; mechanical property

check for updates

Citation: Wang, H.; Wang, Z.; Ding, S.; Jin, C.; Zhang, X.; Liu, L. A Laboratory-Scale Numerical Investigation of the Effect of Confinement Conditions on the Mechanical Responses of Coal under Various Saturation Conditions. *Processes* **2023**, *11*, 3224. https://doi.org/10.3390/pr11113224

Academic Editors: Abbas Abbaszadeh Shahri and Mahjoub Himi

Received: 20 October 2023
Revised: 6 November 2023
Accepted: 8 November 2023
Published: 14 November 2023

1. Introduction

The excessive burning of fossil fuels has led to a significant increase in the concentration of carbon dioxide in the atmosphere [1]. The rise in CO_2 levels is the primary driver for climate change, which in turn is impacting extreme weather events globally [2–4]. To mitigate climate change, carbon storage in deep underground formations has emerged as a potential solution. One approach involves injecting CO_2 into coal seams, which has been tested in laboratories and field trials to assess its effectiveness for sequestration purposes [5–10]. During the sequestration process, the interaction between injected CO_2 and the coal mass leads to notable changes in the hydro-mechanical properties of the coal [11,12]. For example, Viete and Ranjith conducted an experiment where low-rank brown coal samples were pressurized with 1.5 MPa CO_2. They observed a significant strength reduction of approximately 13% [13]. Deep coal seams are commonly favored as storage sites for CO_2 injection, where CO_2 exists in a super-critical state, surpassing its critical pressure of 7.38 MPa and critical temperature of 31.8 °C. Consequently, it is crucial to assess the mechanical behavior of coal under super-critical CO_2 saturation. Ranathunga et al. conducted experiments using brown coal samples saturated with both sub-critical and super-critical CO_2 (up to 10 MPa). They observed a substantial reduction in coal's uniaxial compressive strength (UCS), up to 61.25% [14]. Similarly, Zhang et al. investigated the effect of CO_2 saturation on high-rank coal samples under similar conditions and found a reduction in UCS values of up to 62.71% [15]. In addition to CO_2 saturation, coal seams are inherently saturated with formation water. These researchers also investigated the effect of introducing water into the CO_2 saturation scenario, and they found even greater reductions in strength. However, it should be noted that all the aforementioned studies were conducted under unconstrained environments. While UCS testing offers a straightforward experimental procedure, the results may not fully capture the complex variations in coal's mechanical properties under real in situ conditions. This is particularly relevant when evaluating the impact of CO_2 adsorption, as gas adsorption onto solids is highly dependent on stress conditions [16]. Therefore, further research is necessary to investigate the influence of confining stress on coal samples saturated with CO_2 in order to gain a comprehensive understanding of how confining stress affects the mechanical properties of CO_2-saturated coal.

Pan et al. specifically examined the bulk modulus of high-rank bituminous coal cores under confinement with CO_2 saturation. Their findings indicated that the softening effect of CO_2 adsorption on coal was not clearly evident, except in cases where the samples were saturated under 10 MPa CO_2, which exhibited a reduction in their bulk modulus of approximately 10–20% [17]. In a study by Masoudian et al., sub-critical CO_2 saturation was performed on high-rank coal samples under different confining pressures ranging from 0 to 5.5 MPa. The results showed a reduction in strength of up to approximately 20% in the CO_2-saturated coal samples [18]. According to Zhang et al., they observed an enhancement in both the strength reduction and Young's modulus reduction of coal samples upon CO_2 adsorption [8], which exhibited greater effects in comparison to low-rank coal under similar operating conditions [14]. However, it is worth noting that the strength reduction and Young's modulus reduction appeared to be less pronounced when confining pressure was applied, as observed in the UCS values obtained from Zhang et al.'s study [15]. Indeed, the change in effective stress, as influenced by the application of confining pressure, plays a significant role in affecting the alteration of coal's mechanical properties due to CO_2 adsorption. According to Wang et al. and Dutka, when external stress is introduced, the volume of CO_2 adsorption onto coal is reduced. Furthermore, this reduction becomes more significant with increasing effective stress. These findings suggest that the application of external stress affects the amount of CO_2 that can be adsorbed by coal, with higher effective stress leading to a decrease in CO_2 adsorption volume [16,19]. However, the limited number of studies described above were all conducted under low confining pressure (less than 15 MPa) due to experimental equipment limitations, safety concerns, and the significant time required for fluid saturation under high effective stress. To overcome these limitations, numerical simulation can be employed. By utilizing experimental data obtained from experiments conducted under low stress conditions, the numerical model can be calibrated and validated. Once validated, this model can then be extended to higher stress conditions commonly encountered in the field, facilitating the prediction of coal's mechanical variation. Additionally, the use of numerical models offers time efficiency since they can be easily replicated for various test parameters, unlike laboratory tests which typically demand extensive hours of experimentation.

Several numerical simulation studies on CO_2 storage in coal seams have utilized different simulators [20–24]. For example, Guo et al. proposed a discrete element model to investigate the stress–strain behavior of coal particles under biaxial shear loading. Their simulation revealed strain-softening and volumetric shrinkage behaviors [20]. Masum et al. developed a bespoke model within a coupled thermos-hydro-chemical-mechanical framework to study sub-critical CO_2 storage in deep coal deposits. They predicted a permeability reduction of approximately 17%, which suggests a favorable injection scenario for shallow in situ testing [21]. The nonlinear stress–strain relationship of coal due to CO_2 adsorption was modelled using an elastic damage constitutive model based on the continuum thermodynamics theory [22]. The dynamic mechanical properties and crack propagation behaviors of coal were simulated by developing a numerical model based on bond-based Peridynamic theory, and the stress–strain fields were determined under a split Hopkinson pressure bar system [23]. Ma et al. conducted experiments to evaluate the influence of loading rate on coal mechanics. The experimental results were simulated using the particle flow code, and the careful selection of a suitable material constitutive model ensured a close agreement between laboratory and numerical findings [24]. Vishal et al. employed COMET3 to investigate the CO_2 storage potential of coal seams [25]. Pan and Connell [26] compared simulation results using SIMEDII and TOUGH2 to assess the permeability variation of coal seams upon CO_2 injection [27]. Fan et al. developed a thermo-hydro-mechanical-chemical coupled model solved using COMSOL Multiphysics to examine methane production and CO_2 storage behaviors in coal [28]. However, all these studies primarily focused on the macro-scale, whereas investigations on a laboratory scale, which can directly incorporate experimental inputs, are equally important. Moreover, extending the simulation results of laboratory-scale models to field-scale models can yield valuable insights into the interactions between CO_2 and the coal mass. Therefore, this study aims to develop a laboratory-scale model to simulate the influence of applied stress on coal mechanics during the CO_2 sequestration process with input derived from experimental results.

COMSOL Multiphysics is a commercially available software package that employs the finite element method to solve various physics and engineering problems. This user-friendly software offers a traditional physics-based user interface and allows for the development of user-defined physics through partial differential equations (PDEs). It has been extensively utilized in numerous engineering fields, such as structural engineering, fluid transportation, chemical reactions, and electromagnetics. In the present study, a laboratory-scale model was developed using the input parameters from the experimental results of Zhang et al. [8] and Zhang et al. [15]. The effect of applied stress on the alteration of coal's mechanical properties was modelled and verified. Subsequently, the model was applied to higher stress conditions to investigate the coal mass response resulting from various fluid saturation conditions in deep coal seams.

2. Model Development

A two-dimensional axisymmetric finite element model was developed to simulate the effect of applied stress on the mechanical responses of coal under various saturation conditions using the solid mechanics module in the software package of COMSOL Multiphysics. The simulation procedures are illustrated in Figure 1.

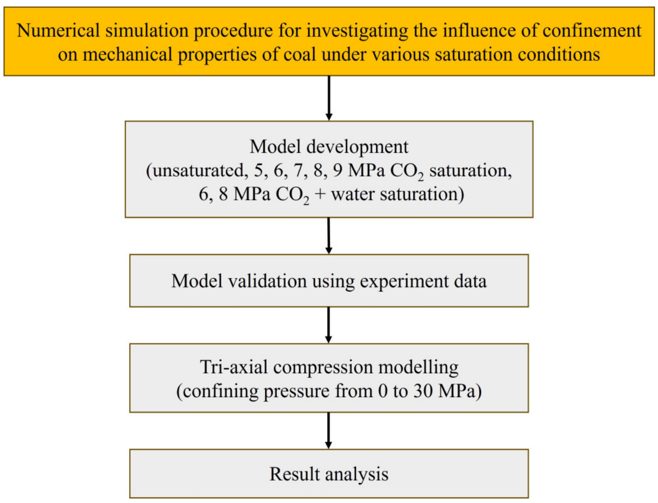

Figure 1. Schematic diagram of the numerical simulation procedures.

2.1. Model Definition and Boundary Conditions

The laboratory experiments involved cylindrical coal samples with a diameter of 38 mm and a height of 76 mm [8]. To account for the axial symmetry of the samples, an axisymmetric model was constructed with a width of 19 mm and a height of 76 mm, as depicted in Figure 2. This validated 2D model can be further extended to a 3D model by revolutionizing the 2D axisymmetric dataset.

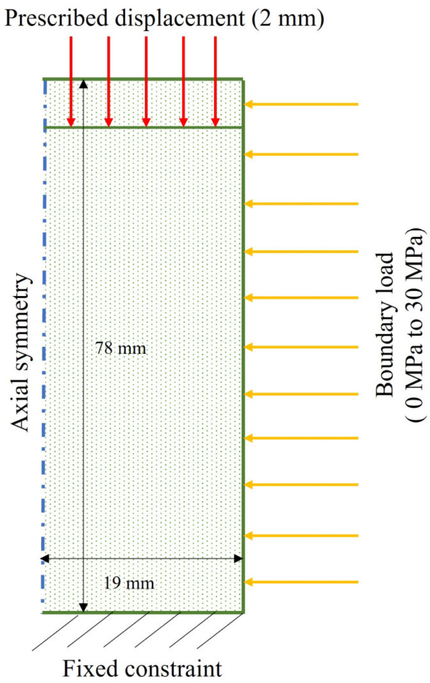

Figure 2. Dimensions and boundary conditions of the numerical model.

The boundary constraints are as follows: (1) a fixed constraint is applied at the bottom of the model; (2) a prescribed displacement is introduced at the top of the model to simulate compression using the auxiliary sweep function; and (3) a boundary load is applied to the circumference of the model in the form of a radial force to account for the confining pressure. The boundary load is adjusted as a parametric sweep, starting from an unconfined condition and gradually increasing to 30 MPa (approximately 1200 m in depth) in 5 MPa increments. Pore pressure can influence the gas adsorption process and the associated volumetric variations [29]. However, it was not considered in the numerical simulation because the adsorption-induced volumetric variation was not included in the current study. The boundary constraints of the developed model are illustrated in Figure 2.

2.2. Governing Equations

In the solid mechanics module, COMSOL defines displacement (u) as the dependent variable. The equations used in solid mechanics are formulated by recording the variation of a certain volume of material as it changes (deforms, rotates, etc.). Therefore, the equations used for deformation analysis in the solid mechanics module are completely Lagrangian, since these equations are derived according to the original configuration of the model. The governing equations for the linear elastic material model are based on Newton's second law of motion:

$$F_v = \rho\left(\frac{\partial^2 u}{\partial t^2}\right) - \nabla\cdot\sigma \tag{1}$$

where F_v is the body force per unit volume, ρ is the density of the material, u(X,t) is the displacement vector, t is the time spent for the particle to move to a new location, and σ is the normal Cauchy stress tensor.

Here, the deformation gradient (∇u) can be calculated as a function of the material coordinates, as indicated in Equation (2):

$$\nabla u = I + \frac{\partial u}{\partial X} \tag{2}$$

where I is the identity tensor and X is the original location of a material particle.

The matrix form of Equation (2) is given as:

$$\nabla \mu = \begin{bmatrix} \frac{\partial x}{\partial X} & \frac{\partial x}{\partial Y} & \frac{\partial x}{\partial Z} \\ \frac{\partial y}{\partial X} & \frac{\partial y}{\partial Y} & \frac{\partial y}{\partial Z} \\ \frac{\partial z}{\partial X} & \frac{\partial z}{\partial Y} & \frac{\partial z}{\partial Z} \end{bmatrix} = \begin{bmatrix} 1 + \frac{\partial u}{\partial X} & \frac{\partial u}{\partial Y} & \frac{\partial u}{\partial Z} \\ \frac{\partial v}{\partial X} & 1 + \frac{\partial v}{\partial Y} & \frac{\partial v}{\partial Z} \\ \frac{\partial w}{\partial X} & \frac{\partial w}{\partial Y} & 1 + \frac{\partial w}{\partial Z} \end{bmatrix} \tag{3}$$

The local rotation and deformation of the material are all given by the deformation gradient. Since the cylindrical coordinate system is adopted in the axial symmetry, the torsional displacement is assumed to be zero, and the radial displacement (u) and axial displacement (w) are considered as two independent variables for axial symmetry. Hence, when the external load is applied to the model, the total Green–Lagrange strain tensor is written in terms of the deformation gradient, as shown in Equation (4):

$$\varepsilon = \frac{1}{2}\left(\nabla u + (\nabla u)^T + \nabla u (\nabla u)^T\right) \tag{4}$$

The constitutive relation between the stress tensor and strain tensor can be described using Hook's law:

$$S = C : \varepsilon \tag{5}$$

where S is the stress tensor, C is the fourth order elasticity tensor, : denotes the double dot tensor product, and ε is the strain tensor.

Since the material is assumed to be linear elastic in this model, the total stress tensor can be related to the strain tensor using Duhamel–Hooke's law, as shown in Equation (6):

$$S - S_0 = C : (\varepsilon - \varepsilon_0 - \varepsilon_{inel}) \tag{6}$$

where S_0 is the initial stress tensor, ε_0 is the initial strain tensor, and ε_{inel} is the sum of all inelastic strains.

The rock sub-node under the linear elastic material node in COMSOL was used to define the properties of the coal sample. The original Hoek–Brown failure criterion, which is a non-linear empirical solution used to describe rock responses under stress conditions, was adopted for this modelling. The material parameters of the rock can be obtained via simple field observation together with the UCS of the intact rock. Therefore, the Hoek–Brown failure criterion for rock mass has been widely adopted by engineers in a large number of applications since the publication of the criterion in 1980 [30]. The Hoek–Brown failure criterion can be expressed as follows:

$$\sigma_1 = \sigma_3 + \sigma_c \left(m \frac{\sigma_3}{\sigma_c} + s \right)^a \tag{7}$$

where $\sigma_1 \geq \sigma_3 \geq 0$ are the principal stresses at failure (σ_1 is the major principal stress and σ_3 is the minor principal stress), σ_c is the uniaxial compressive strength of the intact rock, m, s, a are the positive material parameters, and s equals 1 and a equals 0.5, as intact coal samples are used in the experiment.

With the consideration of the invariants of stress tensor I_1 and J_2, the Hoek–Brown criterion can be expressed as:

$$F_y = 2\sqrt{J_2} \sin\left(\theta + \frac{\pi}{3}\right) - \sigma_c \sqrt{s - m\frac{\sigma_1}{\sigma_c}} = 0 \tag{8}$$

where I_1 is the first invariant of the principal stress tensor (see Equation (9)), J_2 is the second invariant of the deviatoric stress tensor (see Equation (10)), θ is the lode angle (see Equation (11) [31]), and $0 \le \theta \le \pi/3$.

$$I_1 = \sigma_1 + \sigma_2 + \sigma_3 \tag{9}$$

$$J_2 = \frac{1}{2}\mathrm{tr}S^2 = \frac{1}{6}\left[(\sigma_1 - \sigma_2)^2 + (\sigma_1 - \sigma_3)^2 + (\sigma_3 - \sigma_2)^2\right] \tag{10}$$

$$\theta = \arccos\frac{2\sigma_1 - \sigma_2 - \sigma_3}{2\sqrt{3}\sqrt{J_2}} \tag{11}$$

2.3. Basic Assumptions

The following assumptions of the model are made: (1) coal is elastic and isotropic; (2) Hoek–Brown parameters are independent of confining pressure environments and depend only on saturation conditions; (3) the system is isothermal; (4) no moisture or other gas are present in the coal before saturation.

2.4. Model Input Parameters

The material properties for the numerical model were determined based on experimental studies [8,15]. Zhang et al. investigated the variation of coal mechanics by performing a series of uniaxial compressive tests on high-rank bituminous coal samples saturated with CO_2 (2, 4, 6, 8, 10 MPa) and CO_2 (6, 8 MPa) with water [15]. Therefore, the UCS values, Young's modulus, and Poisson's ratios used in the numerical model were derived from the above experiments [15], and the Hoek–Brown parameter m for each saturation condition was obtained from tri-axial tests using the same coal samples [8]. However, since the CO_2 saturation pressures (5, 6, 7, 8, 9 MPa) in the tri-axial tests differed from those in the uniaxial tests, the UCS values, Young's modulus, and Poisson's ratios for 5, 7, and 9 MPa were extrapolated by fitting the corresponding values of the tested samples with the CO_2 saturation pressure, as shown in Figure 3.

Table 1 shows the input parameters for this model.

Table 1. Model input parameters.

Sample Diameter	Sample Length	Density	Confining Pressure	Prescribed Displacement at the Top Boundary
38 mm	76 mm	1450 kg/m^3	0, 5, 10, 15, 20, 25, 30 MPa	2 mm
CO_2 saturation pressure	**Strength (MPa)**	**Young's modulus (GPa)**	**Poisson's ratio**	**Hoek–Brown parameter m**
0	46.07	5.41	0.263	0.419
5 MPa	28.86	4.70	0.297	2.742
6 MPa	26.33	4.58	0.298	3.278
7 MPa	22.85	4.52	0.317	4.292
8 MPa	19.00	4.43	0.331	5.651
9 MPa	18.60	4.35	0.336	5.520
6 MPa + water	23.90	4.45	0.321	3.786
8 MPa + water	14.53	4.33	0.364	7.361

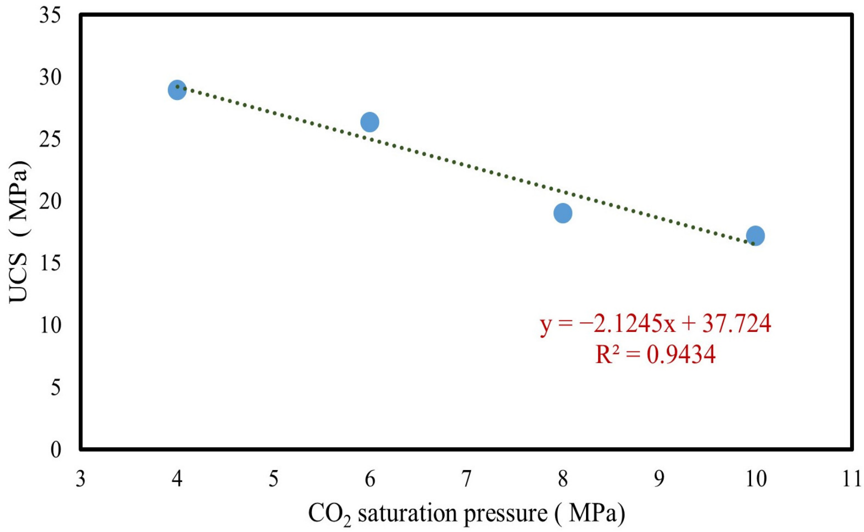

(**a**)

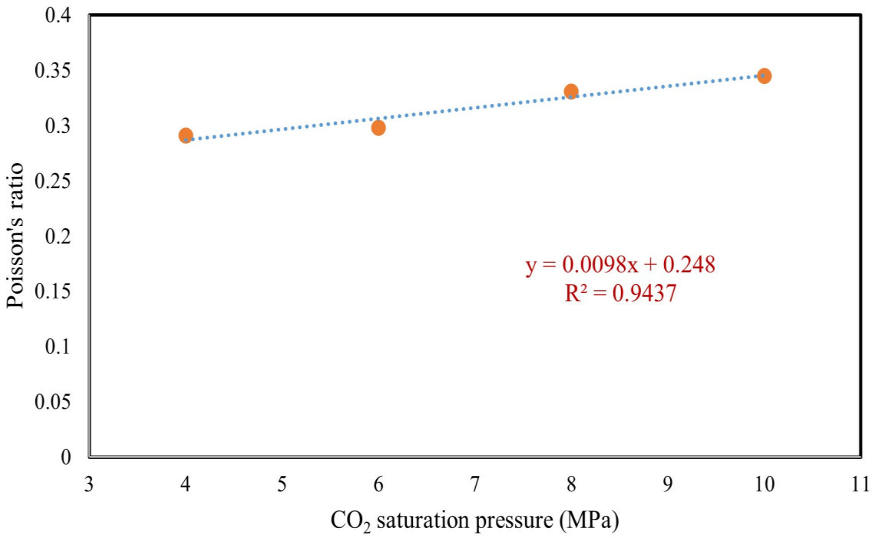

(**b**)

Figure 3. Relationship between CO_2 saturation pressure and (**a**) UCS value of coal and (**b**) Poisson's ratio for coal (from Zhang et al. [15]).

2.5. Meshing and Element Size

A predefined 2D-mapped extremely fine quadrilateral mesh consisting of 2500 domain elements and 250 boundary elements was used for the model, as it is bounded by four boundary segments with no isolated or embedded vertices or segments. Mesh quality was evaluated based on the skewness, which measures equiangular skew. Figure 4 illustrates the mesh quality, with a color range close to 0 indicating poor mesh quality and a color range close to 1 indicating good mesh quality. The average mesh quality for this model is 1.0, which suggests that the assigned mesh fits the model geometry well.

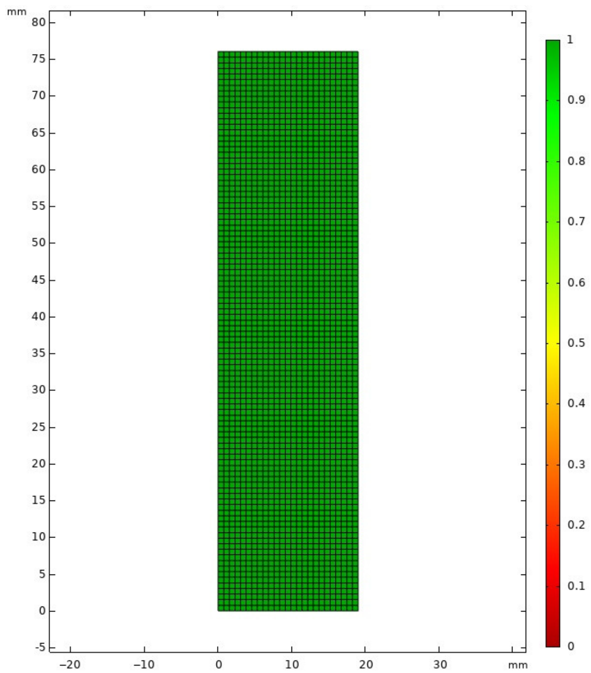

Figure 4. Mesh quality of model.

3. Mechanical Characteristics of Coal under Triaxial Compression

3.1. Model Validation Using Experimental Data

To validate the numerical model, the stress–strain curves obtained from simulation results were compared with the experimental data [8]. In order to calculate the loading stress on the coal sample, an integration node was added on the top boundary of the model to integrate the reaction force over the top boundary. The reaction force can be calculated by

$$F = \int_0^r \sigma 2\pi r dr \tag{12}$$

where F is the reaction force and $2\pi r$ is obtained from the integration of the nodes over the top surface of the model.

Next, the extra loading stress σ_d due to compression was obtained by subtracting the confining pressure from the resulting stress, as indicated in Equation (13):

$$\sigma_d = \frac{F}{\pi R^2} - P_c \tag{13}$$

where R is the radium of the model and P_c is the confining pressure.

The axial strain (ε) of the sample can be directly calculated using the prescribed displacement at the top surface over the sample length, as indicated in Equation (14). The prescribed displacement (Disp) used in this model is applied as an auxiliary sweep from 0 to 2 mm with 0.05 mm intervals.

$$\varepsilon = \frac{Disp}{L} \tag{14}$$

where L is the sample length (76 mm).

Figure 5 depicts a comparison of the stress–strain curves for coal saturated at different CO_2 pressures, demonstrating the agreement between the developed model and experimental results. Notably, the test did not consider post-failure characteristics, as all coal samples exhibited brittle responses after peak stress.

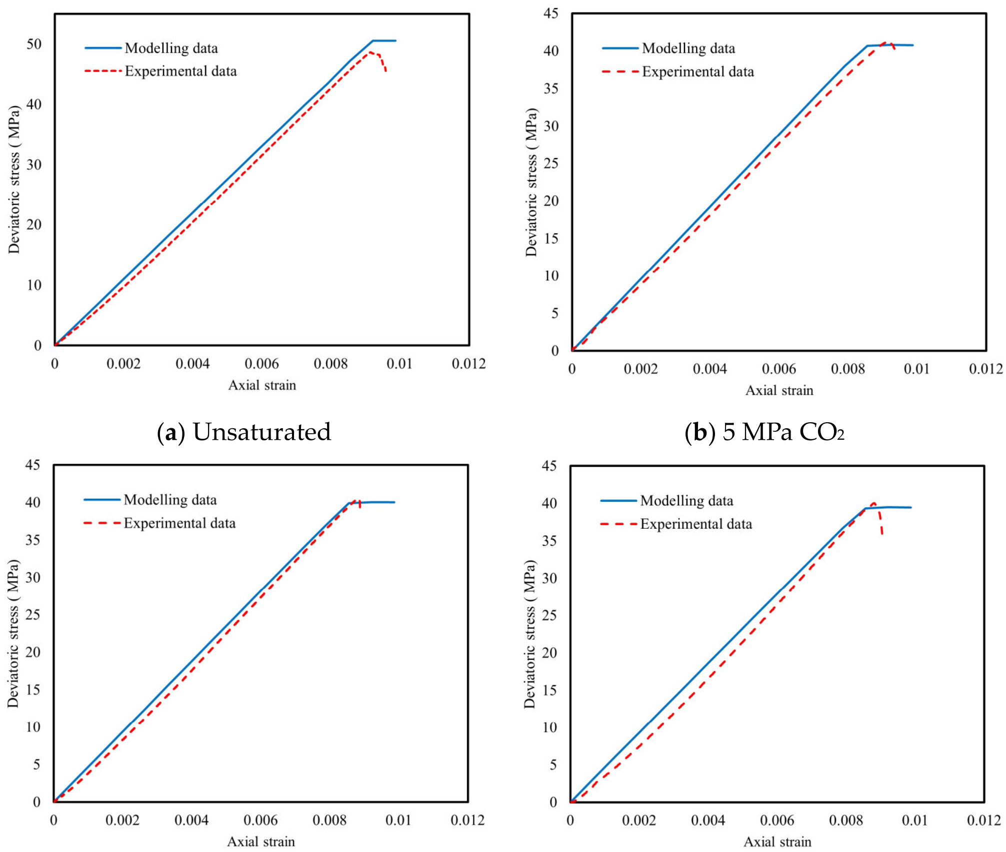

(**a**) Unsaturated (**b**) 5 MPa CO_2

(**c**) 6 MPa CO_2 (**d**) 7 MPa CO_2

Figure 5. Comparison of experimental results and modelling results of stress–strain curves for high-rank bituminous coal either unsaturated (**a**), or under 5 MPa (**b**), 6 MPa (**c**), and 7 MPa (**d**) CO_2 saturation.

3.2. Modelling Results and Discussion

Following the model validation, a parametric sweep from 5 MPa to 30 MPa (approximately 200 m to 1200 m) was conducted to investigate how various confining pressures affect the mechanical response of coal under different saturation conditions. During modelling, the convergence of the model to satisfactory criteria was monitored through the residual plot to examine the stability and accuracy of the numerical solution. Tables 2 and 3 present the modeling results of coal failure strength under different confining stresses and saturation conditions. In this context, "stress" pertains to deviatoric stress.

Table 2. Failure strength for samples (unsaturated, 5, 6, 7 MPa CO_2-saturated) under different confining pressures.

Confining Pressure	Failure Strength of Sample			
	Unsaturated	**5 MPa CO_2**	**6 MPa CO_2**	**7 MPa CO_2**
5 MPa	46.78 MPa	34.64 MPa	33.12 MPa	31.39 MPa
10 MPa	47.79 MPa	39.84 MPa	38.99 MPa	38.28 MPa
15 MPa	48.78 MPa	44.41 MPa	44.07 MPa	44.07 MPa
20 MPa	49.74 MPa	48.60 MPa	48.61MPa	49.21 MPa
25 MPa	50.69 MPa	52.42 MPa	52.79 MPa	53.86 MPa
30 MPa	51.62 MPa	55.99 MPa	56.65MPa	58.13 MPa

Table 3. Failure strength for samples (8, 9 MPa CO_2, 6 MPa + water, 8 MPa + water) under different confining pressures.

Confining Pressure	Failure Strength of Sample			
	8 MPa CO_2	**9 MPa CO_2**	**6 MPa CO_2 + Water**	**8 MPa CO_2 + Water**
5 MPa	29.54 MPa	28.89 MPa	31.55 MPa	26.87 MPa
10 MPa	37.34 MPa	36.52 MPa	37.93 MPa	35.24 MPa
15 MPa	43.79 MPa	42.82 MPa	43.35 MPa	41.96 MPa
20 MPa	49.39 MPa	48.30 MPa	48.18 MPa	47.73 MPa
25 MPa	54.44 MPa	53.23 MPa	52.55 MPa	52.90 MPa
30 MPa	59.06 MPa	57.75 MPa	56.62 MPa	57.61 MPa

Tables 2 and 3 reveal an increase in deviatoric stress at failure with rising confining stress, although the rate of increase diminishes for higher confining stress conditions. For instance, Table 4 illustrates the incremental rate of deviatoric stress in response to different confining pressures for unsaturated samples. A 2.16% increase in deviatoric stress was observed when the confining pressure rose from 5 MPa to 10 MPa, whereas a comparatively smaller increment of 1.84% occurred when the pressure increased from 25 MPa to 30 MPa. This disparity can be attributed to the significant dilation of the sample in lower confining pressure environments, which decreases with increasing confining pressure [32]. Dilatancy is a critical factor governing the generation and propagation of micro-cracks that lead to macroscopic shear crack propagation [33]. Samples subjected to lower confining pressures experience easier generation and the propagation of micro-cracks. Consequently, with increasing confining pressure, the deviatoric stress rises. This suggests that the deviatoric stress of coal is less influenced by deep-buried conditions, highlighting the limited impact of confining pressure on deviatoric strength enhancement in highly confined conditions. Therefore, the overall strength of coal is predominately governed by the confining pressure in deep-buried environments.

Table 4. Variation of deviatoric stress with confining stress for unsaturated samples.

Stress Variation	Increase of Deviatoric Stress at Failure
From 5–10 MPa	2.16%
From 10–15 MPa	2.07%
From 15–20 MPa	1.99%
From 20–25 MPa	1.91%
From 25–30 MPa	1.84%

The impact of confining stress on the deviatoric stress increment in coal exposed to sub-critical and super-critical CO_2 was then investigated. To represent sub-critical and super-critical CO_2 saturation, the samples saturated with 6 MPa CO_2 and 8 MPa CO_2 were selected, respectively. Table 5 displays the model results depicting the variation of deviatoric stress with confining pressure for the 6 MPa and 8 MPa saturated coal samples. According to Table 5, although the deviatoric stress increment at failure in CO_2-saturated samples decreases with increasing confining pressure, the rate of increase in each stage is significantly higher compared to unsaturated samples. For instance, an increase in confining pressure from 5 MPa to 10 MPa induces a 2.16% increase in deviatoric stress for unsaturated coal samples, while the corresponding increments for 6 MPa and 8 MPa CO_2-saturated coal samples are approximately 17.73% and 26.42%, respectively. These findings suggest that changes in confining pressure have a greater impact on the mechanical properties of CO_2-treated coal samples. Experimental studies have confirmed that CO_2 adsorption in the coal mass reduces its strength by reorganizing the coal structure from an initially strained state to a more relaxed state with lower surface tension [8,15,34]. This weakened coal mass is more vulnerable to changes in the confining pressure environment, resulting in a greater increase in deviatoric stress as confining pressure rises. This effect is more pronounced in coal samples saturated at higher CO_2 pressures, as shown in Tables 2 and 3 and Table 5. Higher CO_2 pressures allow more CO_2 molecules to infiltrate the coal mass [35], leading to a greater weakening effect and a higher rate of deviatoric stress increment.

Table 5. Variation of deviatoric stress with confining stress for 6 MPa and 8 MPa CO_2 saturated samples.

Stress Variation	Increase of Deviatoric Stress at Failure	
	6 MPa CO_2	8 MPa CO_2
From 5–10 MPa	17.73%	26.42%
From 10–15 MPa	13.03%	17.25%
From 15–20 MPa	10.29%	12.80%
From 20–25 MPa	8.61%	10.22%
From 25–30 MPa	7.30%	8.49%

Table 6 showcases the increase in deviatoric stress at failure for coal samples saturated with CO_2 + water. Upon comparing the results in Tables 5 and 6, it can be concluded that the rate of deviatoric stress increment at failure with confining pressure is further enhanced for CO_2 + water-saturated coal samples compared to the corresponding CO_2-saturated samples. For instance, the rate of the deviatoric stress increment increases from 17.73% for a 6 MPa CO_2-treated coal sample to 20.21% for a 6 MPa CO_2 + water-treated coal sample when the confining pressure rises from 5 to 10 MPa. Similarly, a 31.13% increment rate is observed for an 8 MPa CO_2 + water-treated coal sample, whereas an increment of 26.42% is measured for an 8 MPa CO_2-treated coal sample with the same variation of confining pressure. As previously mentioned, the adsorption of CO_2 into the coal mass weakens its strength by altering the coal's structure. This weakening effect is further intensified when water is introduced during CO_2 saturation, as the dissolution of CO_2 in water generates acidic carbonate solutions that interact with minerals in the coal, leading to their leaching out. Consequently, the coal strength is reduced. Therefore, a CO_2 + water-saturated coal sample is more susceptible to the influence of confining pressure.

Table 6. Variation of deviatoric stress with confining stress for CO_2 + water saturated samples.

Stress Variation	Increase of Deviatoric Stress at Failure	
	6 MPa CO_2 + Water	8 MPa CO_2 + Water
From 5–10 MPa	20.21%	31.13%
From 10–15 MPa	14.31%	19.07%
From 15–20 MPa	11.14%	13.76%
From 20–25 MPa	9.08%	10.81%
From 25–30 MPa	7.73%	8.90%

Figure 6 illustrates the relationship between deviatoric stress at failure and confining pressure for unsaturated and CO_2-saturated coal samples. The figure shows that the deviatoric stress at failure increases with increasing confining pressure for both unsaturated and CO_2-saturated coal samples. However, the slopes of the curves for the CO_2-saturated samples are much steeper compared to the unsaturated sample, indicating that confining pressure has a greater effect on the strength of the CO_2-saturated coal samples. Moreover, the deviatoric stress at failure decreases with increased CO_2 saturation at lower confining pressures. For instance, under a 5 MPa confining pressure, the deviatoric stress for the unsaturated coal sample is approximately 46.78 MPa. However, it reduces to 33.12 MPa and 29.54 MPa for the 6 MPa and 8 MPa CO_2-saturated coal samples, respectively. Interestingly, this reduction in deviatoric stress due to CO_2 adsorption diminishes with increasing confining pressure, as shown in Figure 6. At some point, the deviatoric stresses of samples saturated at different CO_2 saturation pressures converge under a certain confining pressure.

This critical confining pressure is estimated to be around 20 MPa, indicating that the impact of CO_2 adsorption on coal integrity is insignificant under such confining conditions or burial depths. In this range, the strength of the coal mass is primarily controlled by the applied confining stress.

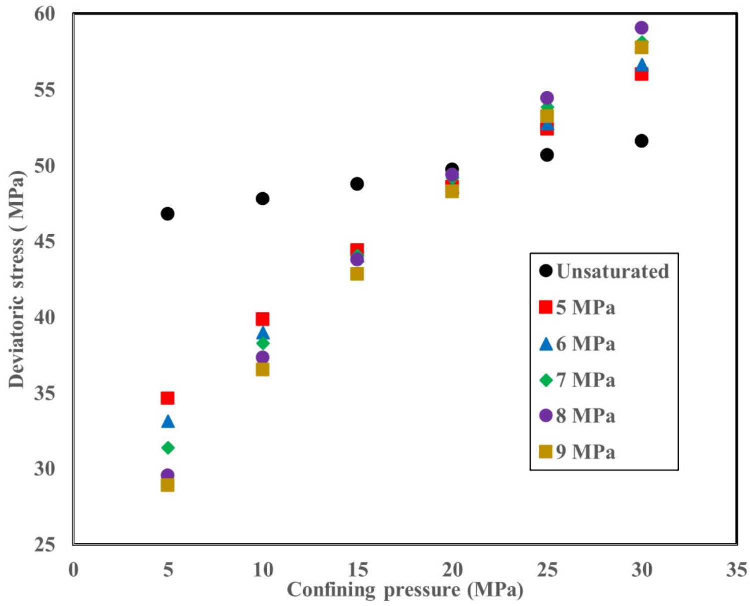

Figure 6. Variation of deviatoric stress at failure with confining pressure for unsaturated and CO_2-saturated coal.

Once this critical confining pressure is exceeded, the CO_2-saturated samples exhibit higher failure stress than the unsaturated sample under the same confining pressure. Additionally, the deviatoric stress of the coal increases with increasing saturation pressure, which is markedly different from the stress behavior observed under low confining pressure. For example, under a 30 MPa confining pressure, the deviatoric failure stress of the unsaturated coal sample is approximately 51.62 MPa. However, it increases to 56.64 MPa and 59.06 MPa for the 6 MPa and 8 MPa CO_2-saturated coal samples, respectively. This suggests that a high confining pressure environment can significantly enhance the strength of a weak coal mass, and the reduction in coal strength caused by CO_2 adsorption becomes negligible at greater burial depths or higher confining pressures.

Figure 7 compares the deviatoric stress for CO_2-saturated and CO_2 + water-saturated coal models under different confining pressures. Introducing water into the CO_2 saturation condition causes a reduction in coal strength, particularly in lower confining pressure environments when compared to single CO_2 saturation. Figure 7 demonstrates that the reduction in strength is more pronounced for 8 MPa CO_2 + water saturation. As the confining pressure increases, the difference in failure values between CO_2 + water-saturated coal and CO_2-saturated coal decreases. For instance, at 5 MPa confining pressure, the failure stress difference between 8 MPa CO_2-saturated and 8 MPa CO_2 + water-saturated coal is 2.67 MPa. However, this difference decreases to 1.46 MPa at 30 MPa confining pressure. Nevertheless, it is important to note that, in this study, the failure deviatoric stress of the CO_2 + water-saturated coal sample is consistently lower than that of the corresponding CO_2-saturated samples, even under a 30 MPa confining pressure, as shown in Figure 7. This indicates that although applying confining pressure improves the strength of a weak coal mass, significantly weakened coal under CO_2 + water saturation may require a higher confining pressure environment to enhance its strength.

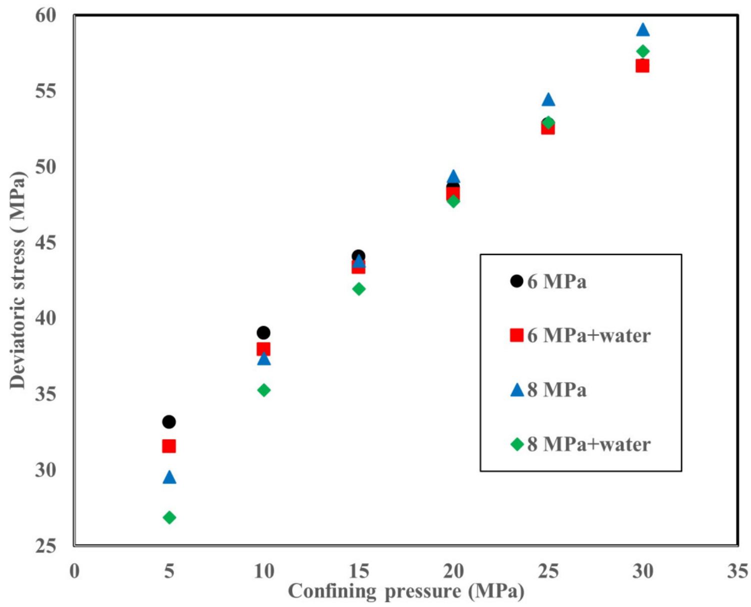

Figure 7. Variation of deviatoric stress with confining pressure for CO_2 saturated and CO_2 + water-saturated coal.

To further investigate this trend, Figure 8 presents the failure stress difference between CO_2-saturated coal samples and their corresponding CO_2 + water-saturated coal samples. As mentioned earlier, the 6 MPa and 8 MPa cases both display decreases in their failure stress differences. The disparity in stress difference between the two cases becomes more pronounced with increasing confining stress. This is primarily due to the relatively large stress difference for the 8 MPa CO_2 case (1.46 MPa at 30 MPa confining pressure), while for the 6 MPa CO_2 case, the stress difference decreases noticeably (0.03 MPa at 30 MPa confining pressure). This highlights the need for a greater confining pressure environment to enhance the strength of 8 MPa + water-saturated coal samples.

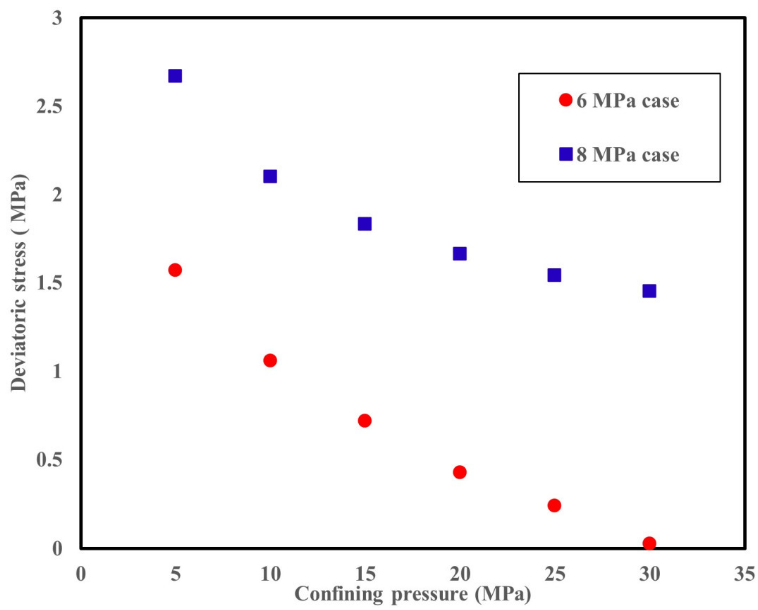

Figure 8. Failure stress difference between CO_2 + water-saturated coal samples and their corresponding CO_2-saturated coal samples with confining pressure.

4. Implications for Field Projects and Future Recommendations

Operational locations for CO_2 sequestration projects often prefer deep-buried coal seams due to the lower risk of CO_2 back-migration into the atmosphere. These deep underground seams are characterized by high stress conditions that can have a positive impact on coal strength. The findings of this study indicate that coal strength increases with higher confining pressures. This effect is particularly evident for coal adsorbed with CO_2, especially at higher CO_2 pressures. This suggests that the weakening effect of CO_2 adsorption in deep underground conditions is significantly outweighed by the mechanical strengthening effect of confinement. Consequently, a higher CO_2 injection pressure is favored not only for its greater adsorption capacity but also for its reduced CO_2 adsorption-induced weakening effect on the coal mass. The study also examined the effect of confining pressure on the strength of CO_2 + water-saturated coal samples, which better simulate the actual underground saturation conditions of coal. Similar results were obtained, demonstrating that the significantly weaker coal mass under CO_2 + water saturation experiences the most significant strength gain when subjected to confining pressure. Therefore, this study's results strongly support the preference of CO_2 sequestration projects in deep coal seams to operate with high CO_2 injection pressures. The input parameters (UCS, Young's modulus, Poisson's ratio, Hoek–Brown parameters) of the current model were directly derived from experimental studies, with the confining pressure being the only variable considered. Hence, a sensitivity analysis was not conducted. However, it is acknowledged that conducting sensitivity and uncertainty analyses will be crucial when multiple variables are introduced to the model. These analyses can help understand the impact of variations in the material properties, geometry, and boundary conditions on the model response, identify critical factors and uncertainties, and make informed decisions to mitigate these uncertainties [36–38]. Indeed, the current study focused on a linear elastic numerical model for evaluating the effects of confining pressure on the mechanical properties of coal with varying CO_2 and water saturation conditions. While this model provides valuable insights, some limitations, as mentioned, could be addressed in future research. Some recommendations for enhancing future modeling efforts are as follows:

- Incorporate a more accurate and realistic material model that captures the stress softening and fracture behavior of coal. This could involve introducing damage mechanics or plasticity theories to better represent the non-linear behavior of coal, or incorporating crack propagation and post-failure response.
- Investigate the coupled effect of temperature on the mechanical behavior of coal during CO_2 sequestration processes in deep coal seams. This would require incorporating the thermal expansion and contraction of the coal mass, as well as considering the interactions between temperature, confining pressure, and the physical and chemical processes occurring during CO_2 and water saturation.
- Examine the role of cyclic loading and unloading in the mechanical response of coal subjected to CO_2 and water saturation. This could further simulate real-world reservoir conditions, as coal seams experience changes in stress states due to fluid injection and extraction processes during CO_2 sequestration projects.
- Consider the effects of heterogeneity and anisotropy commonly observed in natural coal samples. Models accounting for variations in material properties and strength, as well as incorporating fracture structures, can better represent in situ conditions.

5. Conclusions

In tri-axial rock mechanics laboratory experiments, replicating tests for various conditions typically demands considerable time and effort. This study, therefore, aimed to investigate the impact of confining pressure on the mechanical properties of coal under different CO_2 saturation conditions (5 MPa, 6 MPa, 7 MPa, 8 MPa, and 9 MPa) and CO_2 + water saturation conditions (6 MPa and 8 MPa) using a numerical model developed in COMSOL Multiphysics. The findings led to the following conclusions:

- Coal failure strength increases with a rise in confining stress, irrespective of saturation conditions. This can be attributed to the mechanical strengthening effect resulting from the closure of pre-existing fractures within the sample under high-stress conditions.
- The strengthening effect is more pronounced in lower confining pressure environments, where significant dilation promotes micro-crack generation and propagation, ultimately leading to macroscopic failure for samples subjected to reduced confining pressures. Consequently, confining pressure predominantly governs coal strength in deep-buried environments.
- The influence of confining pressure on strength enhancement is more evident in CO_2-saturated coal samples than in unsaturated samples. Structural rearrangement due to CO_2 adsorption weakens the coal mass, rendering it more susceptible to variations in confining conditions and causing a more substantial increase in failure strength as confining pressure increases.
- The strengthening effect of confining pressure on coal rises with increasing CO_2 saturation pressure since coal strength decreases with CO_2 saturation pressure. This effect is further heightened when water is introduced, as acidic carbonate solutions interact with coal minerals, leading to a more significant strength reduction in the coal mass.
- At lower confining pressures, the deviatoric stress at failure declines with increased CO_2 saturation, while it escalates with the rising saturation pressure at higher confining pressures. A critical confining pressure of approximately 20 MPa was identified, under which the failure deviatoric stress of samples saturated with different CO_2 saturation pressures exhibited similar values. In this range, the strength of the coal mass is primarily controlled by the applied confining pressure.

In summary, for CO_2 sequestration projects in deep-buried coal seams involving high-pressure supercritical CO_2 and water, high confining pressure environments can significantly enhance the strength of weak coal masses, rendering the strength reductions caused by CO_2 and water adsorption negligible.

Author Contributions: Conceptualization, H.W. and S.D.; methodology, Z.W. and S.D.; software, X.Z., C.J. and L.L.; writing—original draft preparation, H.W., C.J. and X.Z.; writing—review and editing, Z.W., S.D. and L.L. All authors have read and agreed to the published version of the manuscript.

Funding: This research was funded by National Natural Science Foundation of China (Grant Nos. 42005133, 92162105); Hebei Natural Science Foundation (Grant No. D2022402005); Key Program of Science and Technology Research Project of the Colleges and Universities of Hebei Province (Grant No. ZD2022130).

Institutional Review Board Statement: Not applicable.

Informed Consent Statement: Not applicable.

Data Availability Statement: The data used to support the findings of this study are available from the corresponding author upon reasonable request.

Conflicts of Interest: The authors declare no conflict of interest.

References

1. Perera, F.; Nadeau, K. Climate Change, Fossil-Fuel Pollution, and Children's Health. *N. Engl. J. Med.* **2022**, *386*, 2303–2314. [CrossRef] [PubMed]
2. Ghanbari, M.; Arabi, M.; Georgescu, M.; Broadbent, A.M. The Role of Climate Change and Urban Development on Compound Dry-Hot Extremes across US Cities. *Nat. Commun.* **2023**, *14*, 3509. [CrossRef]
3. Ji, T.; Yao, Y.; Dou, Y.; Deng, S.; Yu, S.; Zhu, Y.; Liao, H. The Impact of Climate Change on Urban Transportation Resilience to Compound Extreme Events. *Sustainability* **2022**, *14*, 3880. [CrossRef]
4. Ukumo, T.Y.; Abebe, A.; Lohani, T.K.; Edamo, M.L. Flood Hazard Mapping and Analysis under Climate Change Using Hydro-Dynamic Model and RCPs Emission Scenario in Woybo River Catchment of Ethiopia. *World J. Eng.* **2023**, *20*, 559–576. [CrossRef]
5. Liu, S.; Liu, T.; Zheng, S.; Wang, R.; Sang, S. Evaluation of Carbon Dioxide Geological Sequestration Potential in Coal Mining Area. *Int. J. Greenh. Gas Control* **2023**, *122*, 103814. [CrossRef]

6. Fujioka, M.; Yamaguchi, S.; Nako, M. CO_2-ECBM Field Tests in the Ishikari Coal Basin of Japan. *Int. J. Coal Geol.* **2010**, *82*, 287–298. [CrossRef]
7. Pan, Z.; Ye, J.; Zhou, F.; Tan, Y.; Connell, L.D.; Fan, J. CO_2 Storage in Coal to Enhance Coalbed Methane Recovery: A Review of Field Experiments in China. *Int. Geol. Rev.* **2017**, *60*, 754–776. [CrossRef]
8. Zhang, X.; Ranjith, P.G.; Lu, Y.; Ranathunga, A.S. Experimental Investigation of the Influence of CO_2 and Water Adsorption on Mechanics of Coal under Confining Pressure. *Int. J. Coal Geol.* **2019**, *209*, 117–129. [CrossRef]
9. Wang, F.; Yan, J. CO_2 Storage and Geothermal Extraction Technology for Deep Coal Mine. *Sustainability* **2022**, *14*, 12322. [CrossRef]
10. Zhang, K.; Liu, H.; Ma, M.; Xu, H.; Fang, H. Multiscale Fractal Characterization of Pore–Fracture Structure of Tectonically Deformed Coal Compared to Primary Undeformed Coal: Implications for CO_2 Geological Sequestration in Coal Seams. *Processes* **2023**, *11*, 2934. [CrossRef]
11. Li, Q.; Wang, F.; Wang, Y.; Forson, K.; Cao, L.; Zhang, C.; Zhou, C.; Zhao, B.; Chen, J. Experimental Investigation on the High-Pressure Sand Suspension and Adsorption Capacity of Guar Gum Fracturing Fluid in Low-Permeability Shale Reservoirs: Factor Analysis and Mechanism Disclosure. *Environ. Sci. Pollut. Res.* **2022**, *29*, 53050–53062. [CrossRef]
12. Li, Q.; Han, Y.; Liu, X.; Ansari, U.; Cheng, Y.; Yan, C. Hydrate as a By-Product in CO_2 Leakage during the Long-Term Sub-Seabed Sequestration and Its Role in Preventing Further Leakage. *Environ. Sci. Pollut. Res.* **2022**, *29*, 77737–77754. [CrossRef] [PubMed]
13. Viete, D.R.; Ranjith, P.G. The Effect of CO_2 on the Geomechanical and Permeability Behaviour of Brown Coal: Implications for Coal Seam CO_2 Sequestration. *Int. J. Coal Geol.* **2006**, *66*, 204–216. [CrossRef]
14. Ranathunga, A.S.; Perera, M.S.A.; Ranjith, P.G.; Bui, H. Super-Critical CO_2 Saturation-Induced Mechanical Property Alterations in Low Rank Coal: An Experimental Study. *J. Supercrit. Fluids* **2016**, *109*, 134–140. [CrossRef]
15. Zhang, X.G.; Ranjith, P.G.; Ranathunga, A.S.; Li, D.Y. Variation of Mechanical Properties of Bituminous Coal under CO_2 and H2O Saturation. *J. Nat. Gas Sci. Eng.* **2019**, *61*, 158–168. [CrossRef]
16. Dutka, B. CO_2 and CH_4 Sorption Properties of Granular Coal Briquettes under in Situ States. *Fuel* **2019**, *247*, 228–236. [CrossRef]
17. Pan, Z.; Connell, L.D.; Camilleri, M. Laboratory Characterisation of Coal Reservoir Permeability for Primary and Enhanced Coalbed Methane Recovery. *Int. J. Coal Geol.* **2010**, *82*, 252–261. [CrossRef]
18. Masoudian, M.S.; Airey, D.W.; El-Zein, A. Experimental Investigations on the Effect of CO_2 on Mechanics of Coal. *Int. J. Coal Geol.* **2014**, *128–129*, 12–23. [CrossRef]
19. Wang, H.; Xiang, J.; Deng, X. Molecular Simulation of the Pore Structure and Adsorption Properties of Coal under Compression Stress. *Energy Fuels* **2023**, *37*, 1887–1895. [CrossRef]
20. Guo, J.; Li, W.; Jiao, Y.; Wang, Y. A Discrete Numerical Simulation of Micromechanics for Dense Coal Granular Systems: Implication for Coal and Gas Outbursts. *Powder Technol.* **2021**, *392*, 448–458. [CrossRef]
21. Masum, S.A.; Chen, M.; Hosking, L.J.; Stańczyk, K.; Kapusta, K.; Thomas, H.R. A Numerical Modelling Study to Support Design of an In-Situ CO_2 Injection Test Facility Using Horizontal Injection Well in a Shallow-Depth Coal Seam. *Int. J. Greenh. Gas Control* **2022**, *119*, 103725. [CrossRef]
22. Xue, Y.; Ranjith, P.G.; Chen, Y.; Cai, C.; Gao, F.; Liu, X. Nonlinear Mechanical Characteristics and Damage Constitutive Model of Coal under CO_2 Adsorption during Geological Sequestration. *Fuel* **2023**, *331*, 125690. [CrossRef]
23. Ai, D.; Zhao, Y.; Wang, Q.; Li, C. Crack Propagation and Dynamic Properties of Coal under SHPB Impact Loading: Experimental Investigation and Numerical Simulation. *Theor. Appl. Fract. Mech.* **2020**, *105*, 102393. [CrossRef]
24. Ma, Q.; Tan, Y.-L.; Liu, X.-S.; Zhao, Z.-H.; Fan, D.-Y.; Purev, L. Experimental and Numerical Simulation of Loading Rate Effects on Failure and Strain Energy Characteristics of Coal-Rock Composite Samples. *J. Cent. South Univ.* **2021**, *28*, 3207–3222. [CrossRef]
25. Vishal, V.; Singh, L.; Pradhan, S.P.; Singh, T.N.; Ranjith, P.G. Numerical Modeling of Gondwana Coal Seams in India as Coalbed Methane Reservoirs Substituted for Carbon Dioxide Sequestration. *Energy* **2013**, *49*, 384–394. [CrossRef]
26. Connell, L.D.; Detournay, C. Coupled Flow and Geomechanical Processes during Enhanced Coal Seam Methane Recovery through CO_2 Sequestration. *Int. J. Coal Geol.* **2009**, *77*, 222–233. [CrossRef]
27. Pan, Z.; Connell, L.D. Impact of Coal Seam as Interlayer on CO_2 Storage in Saline Aquifers: A Reservoir Simulation Study. *Int. J. Greenh. Gas Control* **2011**, *5*, 99–114. [CrossRef]
28. Fan, C.; Elsworth, D.; Li, S.; Zhou, L.; Yang, Z.; Song, Y. Thermo-Hydro-Mechanical-Chemical Couplings Controlling CH_4 Production and CO_2 Sequestration in Enhanced Coalbed Methane Recovery. *Energy* **2019**, *173*, 1054–1077. [CrossRef]
29. Perera, M.S.A.; Sampath, K.H.S.M. Modelling of Free and Adsorbed CO_2-Induced Mechanical Property Alterations in Coal. *Int. J. Coal Geol.* **2020**, *217*, 103348. [CrossRef]
30. Hoek, E.; Brown, E.T. Empirical Strength Criterion for Rock Masses. *J. Geotech. Eng. Div.* **1980**, *106*, 1013–1035. [CrossRef]
31. Jiang, H.; Zhao, J. A Simple Three-Dimensional Failure Criterion for Rocks Based on the Hoek–Brown Criterion. *Rock Mech. Rock Eng.* **2015**, *48*, 1807–1819. [CrossRef]
32. Zhao, X.; Cai, M.; Cai, M. Considerations of Rock Dilation on Modeling Failure and Deformation of Hard Rocks—A Case Study of the Mine-by Test Tunnel in Canada. *J. Rock Mech. Geotech. Eng.* **2010**, *2*, 338–349. [CrossRef]
33. Gowd, T.N.; Rummel, F. Effect of Confining Pressure on the Fracture Behaviour of a Porous Rock. *Int. J. Rock Mech. Min. Sci. Geomech. Abstr.* **1980**, *17*, 225–229. [CrossRef]
34. Li, J.; Pan, J.; Wang, X.; Wang, K.; Nie, S.; Gao, D. Potential Effect of Carbon Dioxide Injection on the Functional Groups of Medium Volatile Bituminous Coals Analysed Using In-Situ Diffuse Reflectance Fourier-Transform Infrared Spectroscopy. *Int. J. Coal Geol.* **2023**, *265*, 104169. [CrossRef]

35. Espinoza, D.N.; Vandamme, M.; Pereira, J.-M.; Dangla, P.; Vidal-Gilbert, S. Measurement and Modeling of Adsorptive–Poromechanical Properties of Bituminous Coal Cores Exposed to CO_2: Adsorption, Swelling Strains, Swelling Stresses and Impact on Fracture Permeability. *Int. J. Coal Geol.* **2014**, *134–135*, 80–95. [CrossRef]
36. Deng, P.; Liu, Q.; Huang, X.; Bo, Y.; Liu, Q.; Li, W. Sensitivity Analysis of Fracture Energies for the Combined Finite-Discrete Element Method (FDEM). *Eng. Fract. Mech.* **2021**, *251*, 107793. [CrossRef]
37. Yang, Q.; Peng, X. Sensitivity Analysis Using a Reduced Finite Element Model for Structural Damage Identification. *Materials* **2021**, *14*, 5514. [CrossRef]
38. Cao, Z.; Fei, Q.; Jiang, D.; Kapania, R.K.; Wu, S.; Jin, H. A Sensitivity-Based Nonlinear Finite Element Model Updating Method for Nonlinear Engineering Structures. *Appl. Math. Model.* **2021**, *100*, 632–655. [CrossRef]